



## Morphological Selection of Gold Nanoparticles Electrodeposited on Various Substrates

Mohamed Saada El-Deab,<sup>a,\*</sup> Tadashi Sotomura,<sup>b</sup> and Takeo Ohsaka<sup>a,\*</sup>

<sup>a</sup>Department of Electronic Chemistry, Interdisciplinary Graduate School of Science and Engineering, Tokyo Institute of Technology, Midori-ku, Yokohama 226-8502, Japan

<sup>b</sup>Matsushita Electric Industrial Company, Advanced Technology Research Laboratory, Seika-cho, Kyoto 619-0237, Japan

Gold nanoparticles with different morphologies (nanocrystallites, perfect nanospheres, plumbs, and nanoaggregates) have been electrodeposited on different substrates, namely, glassy carbon (GC), highly oriented pyrolytic graphite (HOPG), and Au(111) single-crystalline substrates. Au particles with particle size ranging from a few nanometers to a few micrometers have been prepared. The morphology of the electrodeposited Au particles was largely dependent on the nature of the substrate as well as the composition of the electrodeposition bath. For instance, the inclusion of iodide ions during electrodeposition was found to enhance two-dimensional (2D) growth of the Au nanoparticles, and particles with a relatively small particle size down to 10 nm were obtained. The inclusion of L-cysteine (as an additive) during the electrodeposition of the Au nanoparticles resulted in a significant influence on the morphology (and the particle size of the Au particles), which strongly depends on the nature of the substrate. Au nanoparticles with crystalline geometry were prepared on the Au(111) substrates in the presence of L-cysteine, while under the same experimental conditions Au aggregates of size up to 300 nm were electrodeposited on the GC substrates. Au particles with a perfect spherical shape were electrodeposited on the HOPG electrodes. X-ray diffraction measurements of the electrodeposited Au particles revealed significantly different crystallinity of the Au particles and in turn different ratios of the single-crystalline domains constituting the Au particles. The cyclic voltammetric response toward the oxygen reduction reaction at the different Au nanoparticles showed a versatile behavior ranging from a quasi-reversible two-electron reaction to an irreversible overall four-electron reaction in O<sub>2</sub>-saturated 0.5 M KOH solution, demonstrating the entirely different electrocatalytic activity of the thus-prepared Au nanoparticles on different substrates.

© 2005 The Electrochemical Society. [DOI: 10.1149/1.2041948] All rights reserved.

Manuscript submitted March 10, 2005; revised manuscript received June 20, 2005. Available electronically September 21, 2005.

Catalysis and electrocatalysis by nanoparticles have been a subject of continuously growing interest and have been applied for diverse applications<sup>1-26</sup> in which the metal (or metal oxide) nanoparticles are dispersed onto a relatively inert substrate. Au nanoparticle-based catalysts are widely applicable in many vital processes, e.g., reduction of NO with propene, CO or H<sub>2</sub>, removal of CO from H<sub>2</sub> streams, selective oxidation, e.g., oxidation of olefins as well as a selective hydrogenation of CO and CO<sub>2</sub>. In addition to their extraordinary catalytic activity for oxygen reduction,<sup>2,3,23,27-31</sup> Au nanoparticle-based substrates have been efficiently utilized for the hydrogenation of unsaturated organics,<sup>19,32</sup> as well as low-temperature oxidation of CO.<sup>9,20,33</sup> Electrochemical deposition,<sup>34,39</sup> as well as several chemical techniques such as sol-gel<sup>40,41</sup> deposition from colloidal suspension,<sup>42-44</sup> is currently in use for the preparation of different metal and metal oxide nanoparticles of different geometries and shapes. The electrochemical deposition technique is of great use because of the facile control of the characteristics of the metal (or the metal oxide) nanoparticles (e.g., mass, thickness, morphology, etc.) by adjusting the current density, bath chemistry, and temperature.<sup>10,35,45</sup> Recently, we have proposed a simple method<sup>2,35</sup> to induce a unique growth orientation of the Au nanocrystals, which is based on the inclusion of some additives to the Au precursor solution (like L-cysteine or iodide ions) during the electrodeposition process of Au nanoparticles onto glassy carbon (GC) substrate.

The present paper aims at monitoring the morphological changes of the Au nanoparticles electrodeposited on different substrates, namely, Au(111), highly oriented pyrolytic graphite (HOPG), and GC electrodes. L-cysteine (or iodide ions) has been utilized as an additive to the electrodeposition bath. X-ray diffraction (XRD) as well as electrochemical characterization of the different Au nanoparticles has been performed. The electrocatalytic activity of the thus-prepared Au nanoparticles toward the oxygen reduction reaction is assessed via the measurement of the cyclic voltammetric (CV) response in O<sub>2</sub>-saturated 0.5 M KOH. The prospective technological

applications of the Au nanoparticles-based electrochemical nanodevices call for precise control of the morphology and size as well as the crystallographic orientation of the prepared electrocatalysts.

### Experimental

GC electrode, HOPG, and Au(111) single-crystalline sheets were used as the working electrodes. The GC electrodes were in the form of disks ( $\phi = 3.0$  mm) sealed in a Teflon jacket having an exposed geometric surface area of 0.07 cm<sup>2</sup>. The HOPG electrodes were fabricated by freshly cleaving HOPG plates (supplied by NT-MDT Co., Russia) and then supporting them on a plastic substrate (the exposed geometric surface area is 0.15 cm<sup>2</sup>). Au(111) electrodes (having a geometric surface area of 0.15 cm<sup>2</sup>) were obtained by carefully cutting a vapor-deposited Au(111) film sheet supported on a plastic substrate (supplied by Tanaka Kikinokoku Co., Ltd., Japan). Spiral Pt wire and an Ag/AgCl/KCl(sat) served as the auxiliary and the reference electrodes, respectively. Prior to electrodeposition of the Au nanoparticles, the GC electrodes were polished with no. 2000 emery paper and then with aqueous slurries of successively finer alumina powder (particle size down to 0.06  $\mu\text{m}$ ) with the help of a polishing microcloth to a mirror finish and sonicated for 10 min in Milli-Q water. HOPG and Au(111) electrodes were subjected to thorough washing with ethanol and Milli-Q water prior to the electrodeposition of the Au nanoparticles. In some experiments, electro-oxidation of the HOPG substrates was performed, prior to the electrodeposition of the Au nanoparticles, by sweeping the potential between -1.0 and +2.0 V vs Ag/AgCl/KCl(sat) at 100 mV s<sup>-1</sup> for 3 or 60 potential cycles in N<sub>2</sub>-saturated 0.5 M H<sub>2</sub>SO<sub>4</sub> using a conventional two-compartment Pyrex glass electrochemical cell. This was done to generate some hydrophilic domains at the HOPG surface (through the electrogeneration of some quinones, hydroxy, and/or carboxylic acid groups) and in turn to investigate the influence of the extent of the hydrophilicity of the substrate on the morphology of the electrodeposited Au nanoparticles.

Au nanoparticles were electrodeposited from acidic solution of 0.5 M H<sub>2</sub>SO<sub>4</sub> containing 1.0 mM Na[AuCl<sub>4</sub>] in the presence or the absence of the additive (0.1 mM of L-cysteine or iodide ions). A potential-step electrolysis technique from 1.1 to 0 V vs Ag/AgCl/KCl(sat) was utilized to perform the electrochemical

\* Electrochemical Society Active Member.

<sup>c</sup> Permanent address: Department of Chemistry, Faculty of Science, Cairo University, Cairo, Egypt.

<sup>z</sup> E-mail: ohsaka@echem.titech.ac.jp

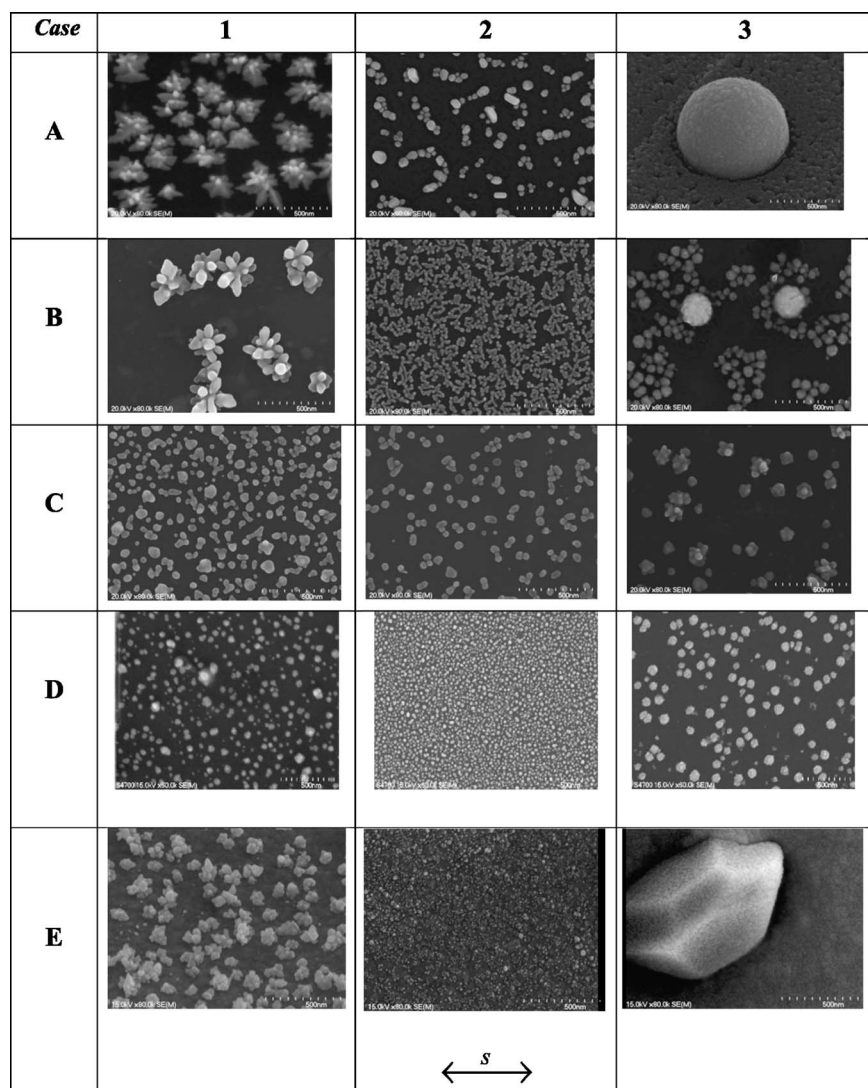


**Figure 1.** SEM images (at magnification factor of 80,000 times,  $s = 500$  nm) of the Au nanoparticles electrodeposited at (A) freshly cleaved untreated HOPG, (B, C) pretreated HOPG substrates, (D) GC electrodes, and (E) Au(111) substrates. Au nanoparticles were electrodeposited onto the different substrates via a potential-step electrolysis from 1.1 to 0 V vs Ag/AgCl/KCl(sat) for 300 s (cases A–C) and 60 s (cases D and E) from acidic solution of 0.5 M  $\text{H}_2\text{SO}_4$  containing 1.0 mM  $\text{Na}[\text{AuCl}_4]$  in the absence (column 1) and the presence of 0.1 mM iodide ions (column 2) and 0.1 mM L-cysteine (column 3). The pretreatment of the HOPG has been performed via sweeping the potential between  $-1.0$  and  $+2.0$  V vs Ag/AgCl/KCl(sat) at  $100 \text{ mV s}^{-1}$  in  $\text{N}_2$ -saturated 0.5 M  $\text{H}_2\text{SO}_4$  for three cycles (case B) and 60 cycles (case C).

deposition of the Au nanoparticles onto the different substrates for different durations using a computer-controlled electrochemical analyzer of BAS 100 B/W.

All chemicals were of analytical grade, supplied by Wako Pure Chemicals Co. (Japan) and were used without further purification.

XRD measurements were performed on a Philips PW 1700 powder X-ray diffractometer, using  $\text{Cu K}\alpha_1$  radiation ( $\lambda = 1.54056 \text{ \AA}$ ), with a Ni filter working at 40 kV and 30 mA. The morphological changes of the different electrodeposited Au nanoparticles on different substrates were depicted from the scanning electron microscopic (SEM) analysis using a JSM-T220 scanning electron microscope (JEOL Optical Laboratory, Japan) at an acceleration voltage of 15 kV and a working distance of 4–5 mm.

### Results and Discussions

*Morphological characterization of the different Au nanoparticles electrodeposited on different substrates.*— Figure 1A–E shows five sets of SEM micrographs obtained for the Au nanoparticles electrodeposited at (A–C) HOPG substrates, (D) GC electrodes, and (E) Au(111) substrates. A freshly cleaved untreated HOPG substrate was used (case A), while a pretreatment of the HOPG has been performed via electro-oxidation in  $\text{N}_2$ -saturated 0.5 M  $\text{H}_2\text{SO}_4$  for three cycles (case B) and 60 cycles (case C). Au nanoparticles were electrodeposited onto the different substrates via a potential-step electrolysis from 1.1 to 0 V vs Ag/AgCl/KCl(sat) for 300 s (cases

A–C) and 60 s (cases D and E) from acidic solution of 0.5 M  $\text{H}_2\text{SO}_4$  containing 1.0 mM  $\text{Na}[\text{AuCl}_4]$  in the absence (column 1) and the presence of 0.1 mM iodide ions (column 2) and 0.1 mM L-cysteine (column 3). Inspection of this figure reveals many interesting morphological features of the Au nanoparticles, i.e.:

The morphology of the Au nanoparticles is largely dependent on the type of the additive present in the electrodeposition bath. For instance, inspect case A which corresponds to Au nanoparticles electrodeposited onto freshly cleaved untreated HOPG substrate. Au aggregates (3D grown) of average particle size of 250 nm were obtained in the absence of any additive (image A-1). A noticeable lowering of the particle size down to 30 nm was observed upon the inclusion of 0.1 mM  $\text{I}^-$  ions to the composition of the electrodeposition bath (image A-2). Interestingly, Au particles with a perfect spherical morphology with a particle size of ca. 700 nm were prepared in the presence of 0.1 mM L-cysteine as an additive (image A-3).

The effect of L-cysteine (as an additive) on the morphology of the Au nanoparticles is significantly dependent on the nature of substrate (see the images along column 3). The size and shape of the perfect spherical nanoparticles prepared on HOPG (image A-3) is distorted in the case of the electrodeposition on the electrochemically three-cycles-treated HOPG substrate (image B-3), and instead of the spherical nanoparticles the formation of Au aggregates predominates at the 60-cycles-treated HOPG substrate (image C-3),

similarly to the electrodeposition on the GC electrodes (image D-3). The presence of L-cysteine induces the formation of Au nanocrystallites (having average diameter of 800 nm) on the Au(111) substrate (image E-3).

Interestingly, the presence of iodide ions induces the formation of small Au nanoparticles of a relatively homogeneous particle size growing in a 2D plane on the different substrates (compare the images along column 2-A-E).

Au nanoparticles electrodeposited onto the HOPG substrates with (image B-1) or without (image A-1) electro-oxidative pretreatment have almost the same morphology (aggregates), indicating the insignificant effect of the mild pretreatment (i.e., three-cycles-treated). The severely pretreated (i.e., 60-cycles-treated) HOPG substrates showed the electrodeposition of Au plumbs (image C-1) almost similar to those obtained at the GC electrodes (image D-1). Thus, the electro-oxidative pretreatment of the HOPG substrate changes it into a GC-like surface while retaining the same degree of substrate crystallinity (cf. Fig. 4B). Thus, the change in morphology of the Au nanoparticles resulting from the electro-oxidation of the HOPG substrates can be safely attributed to a significant change in the surface hydrophilicity rather than its crystallinity.

**Growth modes.**—The different morphologies of the electrodeposited Au nanoparticles under the different operating conditions suggest different forms of growth mechanisms. Generally, the first step of metal deposition is the formation of nuclei of the depositing metal. Subsequently, two competing processes, i.e., the growth and nucleation take place.<sup>46</sup> The relative rate of each process with respect to the other determines the granularity of the deposit. For instance, the higher the nucleation rate of the deposit, the smaller is the crystal size and vice versa.

In particular, in cases with a higher growth rate of the crystal normal to the substrate surface, we may expect the formation of either a fibrous (pin-like) structure of the deposit in the case of a unidirectionally grown deposit<sup>47</sup> or a deposit with largely developed crystal faces parallel to the substrate in the case of a laminar (layer-by-layer) grown deposit.<sup>46</sup>

For the cases at which Au nanoparticles were electrodeposited in the presence of iodide ions (images along column 2 of Fig. 1), a 2D growth mechanism prevails irrespective of the nature of the substrate. That is, the instantaneous adsorption of  $I^-$  ions on the surface of the Au nanoparticles<sup>48</sup> at the early stage of electrodeposition (i.e., at the first formed nuclei) results in the Au nanoparticles with a negative charge. This leads to a repulsive interaction among the negatively charged Au nanoparticles and prevents the further particle growth or the coalescence of the neighboring particles. Thus, the rate of nucleation exceeds the rate of particle growth. Consequently, electrodeposition of Au nanoparticles of small particles size and high particle density predominates.

The growth of the Au nanoparticles excels the nucleation for the Au nanoparticles electrodeposited onto either HOPG, GC, or Au(111) substrates in the presence of L-cysteine as revealed from the relatively big size of the electrodeposited Au nanoparticles (see images along column 3 of Fig. 1). However, the morphology of the electrodeposited Au nanoparticles is entirely different, largely depending on the substrate.

The case of Au nanoparticle/HOPG system represents a weak metal-substrate interaction due to the difference in hydrophilicity of the two phases. Thus, the Au nanoparticles tend to deposit on the HOPG substrate while maintaining the minimum contact area with the substrate and growing homogeneously over the first formed nuclei, leading to the formation of spherical-shape deposit with relatively big size (see image A-3). Note that the first formed nuclei of the metal are normally deposited in the energetically most stable crystallographic orientation [i.e., in the Au(111) in the present case].<sup>46</sup> While the case of the Au nanoparticle/Au(111) system represents a strong metal-substrate interaction. Thus, the deposit tends to have a larger contact area with the substrate. Thus the layer-by-

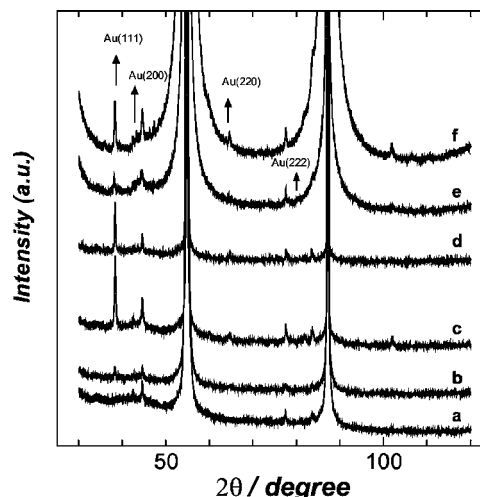


**Figure 2.** XRD patterns of the Au nanoparticles electrodeposited onto freshly cleaved untreated HOPG electrodes (b–f) and for the bare untreated HOPG (a). Electrodeposition of the Au nanoparticles was performed by applying potential-step electrolysis from 1.1 to 0 V vs  $Ag/AgCl/KCl(sat)$  for (b) 60, (c, e, f) 300, and (d) 900 s in acidic solution of 0.5 M  $H_2SO_4$  containing 1.0 mM  $Na[AuCl_4]$  in the absence (b–d) and the presence of (e) 0.1 mM  $I^-$  ions and (f) 0.1 mM L-cysteine.

layer growth mode prevails and ultimately nanocrystallites of Au were formed on the Au(111) substrate (see image E-3). The actual role of L-cysteine is not fully understood at the moment and further investigation is being planned for clarifying this.

**XRD characterization of the different Au nanoparticles electrodeposited on different substrates.**—In order to characterize the crystallographic orientation of the electrodeposited Au nanoparticles, XRD measurements have been performed to monitor the relative distribution of the different facets of the Au single-crystalline domains constituting the Au nanoparticles electrodeposited onto different substrates. Figures 2-6 show typical XRD patterns for the Au nanoparticles electrodeposited on freshly cleaved untreated HOPG (Fig. 2), mildly pretreated HOPG (Fig. 3), severely pretreated HOPG (Fig. 4), GC (Fig. 5), and Au(111) (Fig. 6) substrates, respectively. We cannot compare the intensities of the XRD patterns obtained for the Au nanoparticles electrodeposited on different substrates due to the different background response of each substrate. For instance, we can calculate the crystallographic orientation index ( $N$ ) using the Wilson equation (Eq. 1) for the Au nanoparticles electrodeposited on the well-oriented HOPG substrate, but we cannot compare with that of the Au nanoparticles deposited on the GC substrate due to the higher background response of the GC substrate.

The crystallographic orientation index ( $N$ ) is a measure of the relative ratio of the preferentially formed facets of the Au deposits and is given by<sup>49,50</sup>

$$N = \frac{\frac{III_{(hkl)}}{\sum III_{(hkl)}}}{\frac{JCPDS \cdot III_{(hkl)}}{\sum JCPDS \cdot III_{(hkl)}}} \quad [1]$$

where  $III_{(hkl)}$  is the ratio of diffraction intensities,  $JCPDS \cdot III_{(hkl)}$  is the ratio of diffraction intensities of the JCPDS standard, and the sums represent the combined ratios of the total diffraction intensities for all the crystalline faces. A preferentially formed crystallographic orientation (facet) will have a value of  $N$  higher than 1. If for all the facets a value of  $N = 1$  is obtained, then the deposit has no preferential orientation. Table I summarizes the values of  $N$  of the different facets of the Au nanoparticles electrodeposited on freshly cleaved

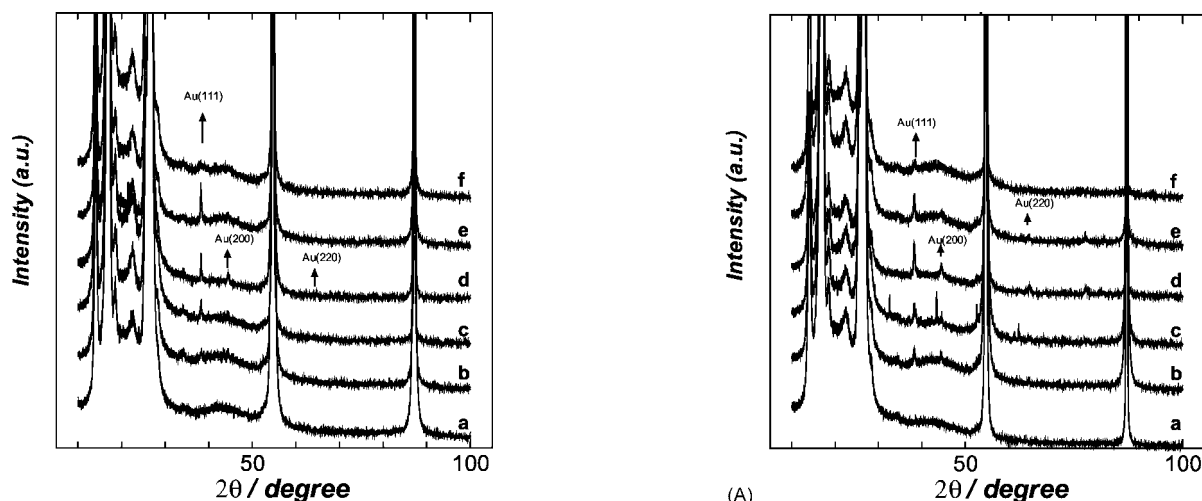


**Figure 3.** XRD patterns of the Au nanoparticles electrodeposited onto pretreated HOPG electrodes (b–f) and for the bare pretreated HOPG (a). Electrodeposition of the Au nanoparticles was performed by applying potential-step electrolysis from 1.1 to 0 V vs Ag/AgCl/KCl(sat) for (b) 60, (c, e, f) 300, and (d) 900 s in acidic solution of 0.5 M H<sub>2</sub>SO<sub>4</sub> containing 1.0 mM Na[AuCl<sub>4</sub>] in the absence (b–d) and the presence of (e) 0.1 mM I<sup>−</sup> ions and (f) 0.1 mM L-cysteine. The HOPG electrodes were subjected to electro-oxidative pretreatment in N<sub>2</sub>-saturated 0.5 M H<sub>2</sub>SO<sub>4</sub> by sweeping the potential between −1.0 and +2.0 V vs Ag/AgCl/KCl(sat) at 100 mV s<sup>−1</sup> for three cycles.

untreated HOPG substrates. In Fig. 2–4, the major peaks located at 2θ of ca. 26.4°, 54.8°, and 87.3° correspond to the C(002), C(004), and C(006) basal planes of the HOPG substrate, respectively. Some other minor peaks located at 2θ of ca. 43.5°, 46.3°, 77.7°, and 83.8° correspond to the C(100), C(101), C(110), and C(112) facets of the HOPG substrate, respectively. Importantly, the peaks located at 2θ of 38.2°, 44.4°, 64.6°, and 81.7° correspond to the Au(111), Au(200), Au(220), and Au(222) facets of the electrodeposited Au nanoparticles, respectively, whereas the peaks in the region of 2θ of 10–22° in Fig. 3 and 4A originate from the plastic support of the HOPG plates. Inspection of Table I (and Fig. 2) reveals the following significant remarks regarding the *N* values of the different facet domains of the electrodeposited Au nanoparticles:

For sample 3 (curve c in Fig. 2), the Au nanoparticles electrodeposited onto the freshly cleaved untreated HOPG in the absence of any additive was found to possess a value of *N* of 2.49 for the Au(111) facet, indicating the preferential electrodeposition of the Au nanoparticles in this crystallographic orientation rather than the Au(200), Au(220), or Au(222) facets. The same result was obtained for the Au nanoparticles electrodeposited for longer electrodeposition time (sample 4, curve d). The Au(111) facet is the thermodynamically most stable facet among the facets of the Au.

The inclusion of I<sup>−</sup> ions to the electrodeposition bath (sample 5, curve e) resulted in a significant decrease of the *N* value of the Au(111) down to 1.26, concurrently with a significant increase in the values of *N* more than unity corresponding to the Au(200) and Au(220) facets and with a slight change in the values of *N* corresponding to the Au(222) facets. This indicates a significant influence of the iodide ions on the preferential distribution of the various single-crystalline domains constituting the Au nanoparticles.

Interestingly, the inclusion of cysteine (sample 6, curve f) favors the formation of the Au(111) along with the Au(220) facet domains of the Au nanoparticles more than the iodide ion does, as can be readily seen from the corresponding values of *N*, while the formation of the Au(222) facet domain is much depressed, as indicated by the low value of the corresponding *N*.

Figures 3 and 4A demonstrate an interesting fact that the electro-oxidative pretreatment has no significant detrimental effect on the

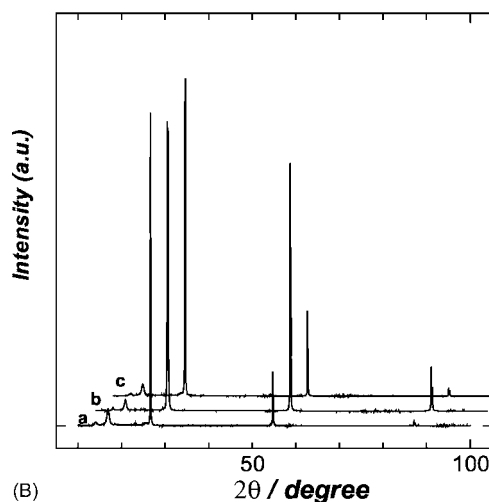


**Figure 4.** (A) XRD patterns of the Au nanoparticles electrodeposited onto pretreated HOPG electrodes (curves b–f) and for the bare pretreated HOPG (curve a). Electrodeposition of the Au nanoparticles was performed by applying potential-step electrolysis from 1.1 to 0 V vs Ag/AgCl/KCl(sat) for (b) 60, (c, e, f) 300, and (d) 900 s in acidic solution of 0.5 M H<sub>2</sub>SO<sub>4</sub> containing 1.0 mM Na[AuCl<sub>4</sub>] in the absence (b–d) and the presence of (e) 0.1 mM I<sup>−</sup> ions and (f) 0.1 mM L-cysteine. The HOPG electrodes were subjected to electro-oxidative pretreatment in N<sub>2</sub>-saturated 0.5 M H<sub>2</sub>SO<sub>4</sub> by sweeping the potential between −1.0 and +2.0 V vs Ag/AgCl/KCl(sat) at 100 mV s<sup>−1</sup> for 60 cycles. (B) XRD patterns of (a) freshly cleaved untreated HOPG and (b, c) pretreated HOPG electrodes. The electro-oxidative pretreatment of the HOPG electrodes was performed in N<sub>2</sub>-saturated 0.5 M H<sub>2</sub>SO<sub>4</sub> by sweeping the potential between −1.0 and +2.0 V vs Ag/AgCl/KCl(sat) at 100 mV s<sup>−1</sup> for (b) 3 and (c) 60 cycles. Note that curves b and c of (B) were shifted by 4 and 8°, respectively, to overcome the peak overlapping with that of curve a.

crystallinity of the HOPG substrate, as can be seen from the existence of the same main peaks at 2θ of ca. 54.8 and 87.3°, corresponding to the C(004) and C(006) domains of the HOPG substrate. Figure 4B compares the XRD patterns of the HOPG substrates subjected to different degrees of electro-oxidative pretreatment. Note that curves b and c of Fig. 4B were shifted by 4° and 8°, respectively, to overcome the peak overlapping. This figure shows that no significant change of the crystallinity of the HOPG substrates was observed upon the electro-oxidative pretreatment as reflected from the existence of the three major peaks located at 2θ of ca. 26°, 54°, and 87°, corresponding to the C(002), C(004), and C(006) basal planes of the HOPG substrate. A most pronounced effect of cysteine (other than that observed in Fig. 2) has been observed in both cases

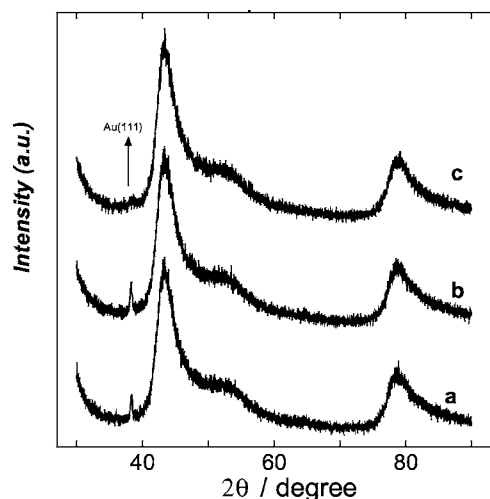


**Figure 5.** XRD patterns of the Au nanoparticles electrodeposited onto GC electrodes ( $\phi = 3.0$  mm) by applying potential-step electrolysis from 1.1 to 0 V vs Ag/AgCl/KCl(sat) for 300 s in acidic solution of 0.5 M  $\text{H}_2\text{SO}_4$  containing 1.0 mM  $\text{Na}[\text{AuCl}_4]$  in (a) the absence of L-cysteine and  $\text{I}^-$  ions and (b) the presence of 0.1 mM  $\text{I}^-$  ions and (c) 0.1 mM L-cysteine.

(i.e., Fig. 3 and 4A). That is, a significant decrease in the peak intensity located at around  $38^\circ$  corresponding to the Au(111) facet domain of the electrodeposited Au nanoparticles prepared in the presence of L-cysteine as an additive has been observed. This peak was much intensified in the presence of iodide ions (compare curves e and f of Fig. 3 and 4A).

Figure 5 shows the XRD patterns of the Au nanoparticles electrodeposited on the GC electrodes in the absence (a) and the presence of (b) 0.1 mM  $\text{I}^-$  ions and (c) 0.1 mM L-cysteine. Obviously, the background response of the GC substrate is high and thus the quantitative estimation of the different facets of the electrodeposited Au nanoparticles is extremely difficult. A noteworthy qualitative observation is that the Au nanoparticles electrodeposited in the presence of iodide ions are much enriched in the Au(111) facet as compared with those prepared in the presence of L-cysteine, as indicated from the relative intensity of the XRD peaks located at  $2\theta$  of ca.

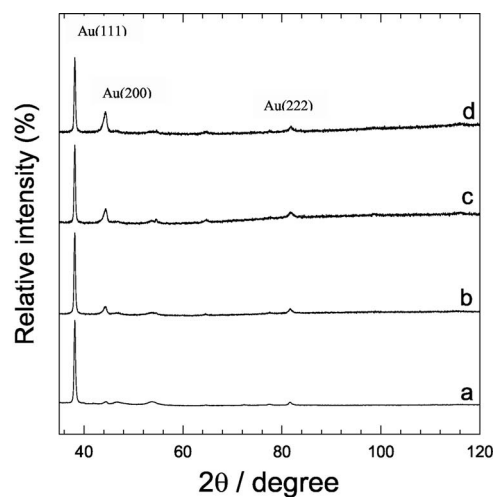


**Figure 6.** XRD patterns of (a) blank Au(111), and (b–d) Au nanoparticles electrodeposited onto Au(111) electrodes by applying potential-step electrolysis from 1.1 to 0 V vs Ag/AgCl/KCl(sat) for 300 s in acidic solution of 0.5 M  $\text{H}_2\text{SO}_4$  containing 1.0 mM  $\text{Na}[\text{AuCl}_4]$  in (b) the absence of L-cysteine and  $\text{I}^-$  ions and (c) the presence of 0.1 mM  $\text{I}^-$  ions and (d) 0.1 mM L-cysteine. The potential was stepped from 1.1 to 0 V for 300 s.

**Table I.** List of the values of the crystallographic orientation index ( $N$ ) of the different single-crystalline facets of the Au nanoparticles electrodeposited on freshly cleaved untreated HOPG substrates.<sup>a</sup>

Sample no.	$2\theta \rightarrow$	$38.18^\circ$	$44.39^\circ$	$64.57^\circ$	$81.72^\circ$
$\downarrow$	Facets $\rightarrow$	$N_{\text{Au}(111)}$	$N_{\text{Au}(200)}$	$N_{\text{Au}(220)}$	$N_{\text{Au}(222)}$
1	Bare HOPG				
2	Nano Au/HOPG	1	...	...	...
3	Nano Au/HOPG	2.49	0.51	0.67	0.33
4	Nano Au/HOPG	2.44	0.49	0.81	0.25
5	Nano Au/HOPG	1.26	1.38	1.28	0.22
6	Nano Au/HOPG	1.55	0.89	1.45	0.09

<sup>a</sup>The data were extracted from Fig. 2. Samples 2–6 correspond to Au nanoparticles electrodeposited onto freshly cleaved untreated HOPG substrates. Electrodeposition was performed from acidic solution of 0.5 M  $\text{H}_2\text{SO}_4$  containing 1.0 mM  $\text{Na}[\text{AuCl}_4]$  in the absence (2–4) and the presence of (5) 0.1 mM  $\text{I}^-$  ions and (6) 0.1 mM L-cysteine, applying potential-step electrolysis from 1.1 to 0 V vs Ag/AgCl/KCl(sat) for (2) 60, (3, 5, 6) 300, and (4) 900 s.

$38^\circ$ . Figure 6 shows the XRD patterns of the Au nanoparticles electrodeposited on the well-oriented Au(111) substrate in the absence (b) and the presence of (c) 0.1 mM iodide ions and (d) 0.1 mM L-cysteine. Note that all the peaks are represented as a relative ratio of the main peak of the Au(111) substrate located at  $2\theta$  of ca.  $38^\circ$ . A close inspection of this figure reveals a significantly high ratio of the Au(200) facet of the Au nanoparticles electrodeposited in the presence of L-cysteine compared with that of the Au nanoparticles prepared in the presence of iodide. Table II summarizes the relative ratio of the different facets of the Au nanoparticles electrodeposited on the Au(111) substrate. The standard ratio of the different facets constituting the usual polycrystalline Au electrode (poly-Au) is also shown for comparison (sample 5). This table shows that the ratio of the Au(200) facet is five times that of the Au(222) facet of the Au nanoparticles electrodeposited in the presence of L-cysteine (sample 4), while the normal ratio of the same two facets is only 1.6 in the polycrystalline Au. This indicates the significant influence of L-cysteine as an additive on the preferential deposition of the Au nanoparticles in the Au(200) orientation. The Au nanoparticles de-

**Table II.** List of the relative peak intensity of the different single-crystalline facets of the Au nanoparticles electrodeposited on Au(111) single-crystalline substrate.<sup>a</sup>

Sample no. $\downarrow$	$2\theta \rightarrow$	$38.18^\circ$	$44.39^\circ$	$81.72^\circ$
	Au(111)	Au(200)	Au(222)	Au(222)
	(%)	(%)	(%)	(%)
1	Au(111)	100%	<2.5%	<2.5%
2	Nano Au/ Au(111)	100%	10%	5%
3	Nano Au/ Au(111)	100%	18%	6%
4	Nano Au/ Au(111)	100%	30% $\rightarrow$	6%
5	Poly-Au	100%	52% $\rightarrow$	32%

<sup>a</sup>The data were extracted from Fig. 6. Sample 1 corresponds to the bare Au(111) single-crystalline substrate, samples 2–4 correspond to Au nanoparticles electrodeposited on Au(111) substrates. Electrodeposition was performed from acidic solution of 0.5 M  $\text{H}_2\text{SO}_4$  containing 1.0 mM  $\text{Na}[\text{AuCl}_4]$  in the absence (2) and the presence of (3) 0.1 mM  $\text{I}^-$  ions and (4) 0.1 mM L-cysteine, applying potential step electrolysis from 1.1 to 0 V vs Ag/AgCl/KCl(sat) for 60 s. Sample 5 corresponds to the usual polycrystalline Au electrode.

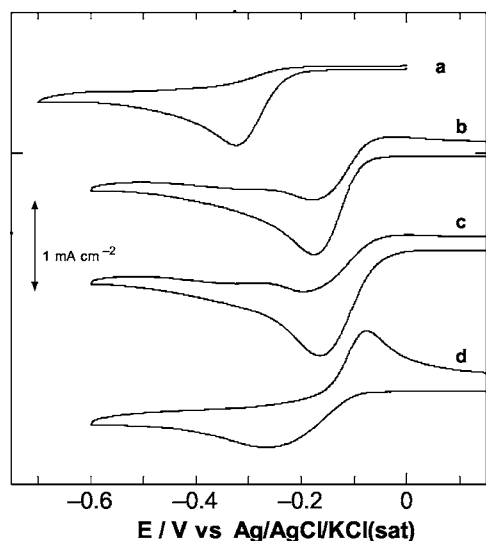


**Figure 7.** CVs for the ORR at (a) bare GC and (b–d) Au nanoparticles electrodeposited onto GC electrodes, measured in  $O_2$ -saturated 0.5 M KOH at potential scan rate of  $100 \text{ mV s}^{-1}$ . The Au nanoparticles were electrodeposited from acidic solution of 0.5 M  $H_2SO_4$  containing 1.0 mM  $Na[AuCl_4]$  in (b) the absence and the presence of (c) 0.1 mM L-cysteine and (d) 0.1 mM  $I^-$  ions by applying a 300 s potential-step electrolysis from 1.1 to 0 V.

posited in the presence of iodide ions showed a less pronounced enrichment in the Au(200) orientation.

**Oxygen reduction.**— The mechanistic pathway of the oxygen reduction reaction, in alkaline media, is known to be very sensitive to the crystallographic orientation of the Au substrate. That is, an Au nanoparticle-based electrode enriched in the Au(111) facet shows a poor electrocatalytic activity, as can be seen from a quasi-reversible two-electron reduction of oxygen to hydrogen peroxide at this electrode.<sup>35,51</sup> An electrode enriched in the Au(100) orientation is shown to support an irreversible four-electron reduction of oxygen to water.<sup>2,35</sup> Thus, in order to assess the electrocatalytic ability of the different Au nanoparticles electrodeposited on GC and untreated and treated HOPG electrodes, the cyclic voltammograms (CVs) shown in Fig. 7–10 were measured in  $O_2$ -saturated 0.5 M KOH at scan rate of  $100 \text{ mV s}^{-1}$ . Figure 7 shows the CVs for the oxygen reduction reaction (ORR) at (a) bare GC and (b–d) Au nanoparticles electrodeposited onto GC electrodes, prepared in the absence (b) and the presence (c) of 0.1 mM L-cysteine and (d) 0.1 mM  $I^-$  ions. A slight positive shift of the cathodic peak potential along with an increase of the peak current was observed for the ORR at Au nanoparticles electrodeposited on the GC electrode in the presence of L-cysteine (curve c). The Au nanoparticles electrodeposited in the presence of iodide ions are considered the least active, as can be seen from a quasi-reversible behavior for the ORR along with a negative shift of the cathodic peak potential and a rather broad and small peak current (curve d). We have shown that the Au nanoparticles electrodeposited in the presence of L-cysteine behave like Au(100) electrodes,<sup>2</sup> being in agreement with the observation deduced from the XRD measurements, which indicated a significantly low ratio of the less active Au(111) facet (see curve c of Fig. 5). Figure 8 shows the CVs of the ORR, measured in  $O_2$ -saturated 0.5 M KOH, at (a) freshly cleaved untreated HOPG and (b–d) Au nanoparticles electrodeposited on the freshly cleaved HOPG electrodes. Au nanoparticles were electrodeposited in the absence (b) and the presence (c) of 0.1 mM L-cysteine and (d) 0.1 mM  $I^-$  ions. This figure shows that the Au nanoparticles deposited on the HOPG electrode in the presence of L-cysteine showed the least activity for the ORR (curve c), in contrast to the Au nanoparticles electrodeposited onto GC electrodes in the presence of L-cysteine (curve c of Fig. 7). That is, the Au nanoparticles electrodeposited onto the freshly cleaved

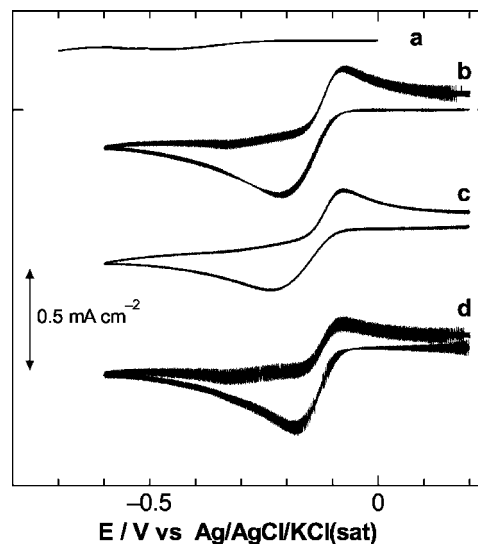


**Figure 8.** CVs for the ORR at (a) freshly cleaved untreated HOPG and (b–d) Au nanoparticles electrodeposited onto freshly cleaved HOPG substrate, measured in  $O_2$ -saturated 0.5 M KOH at potential scan rate of  $100 \text{ mV s}^{-1}$ . The Au nanoparticles were electrodeposited from acidic solution of 0.5 M  $H_2SO_4$  containing 1.0 mM  $Na[AuCl_4]$  in (b) the absence and the presence of (c) 0.1 mM L-cysteine and (d) 0.1 mM  $I^-$  ions by applying a 300 s potential-step electrolysis from 1.1 to 0 V.

untreated HOPG electrodes in the presence of L-cysteine gave a quasi-reversible CV response with the small and broad peak current compared to the Au nanoparticles electrodeposited on the same substrate in the presence of iodide ions (curve d of Fig. 8). This may be explained in view of the relative enrichment in the less active Au(111) orientation of the former electrode (prepared in the presence of L-cysteine) as compared to the latter electrode (prepared in

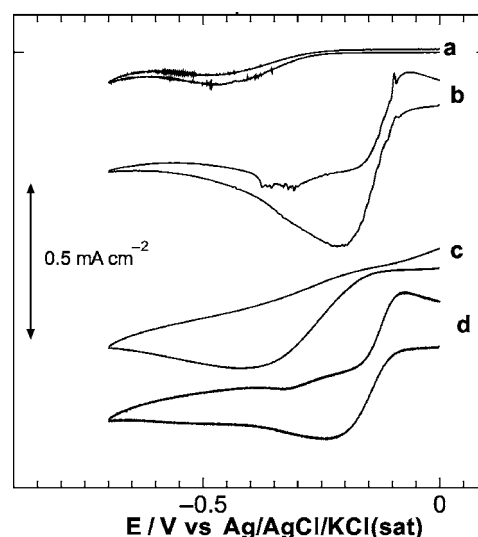


**Figure 9.** CVs for the ORR at (a) pretreated HOPG and (b–d) Au nanoparticles electrodeposited onto pretreated HOPG substrate, measured in  $O_2$ -saturated 0.5 M KOH at potential scan rate of  $100 \text{ mV s}^{-1}$ . The Au nanoparticles were electrodeposited from acidic solution of 0.5 M  $H_2SO_4$  containing 1.0 mM  $Na[AuCl_4]$  in (b) the absence and the presence of (c) 0.1 mM  $I^-$  ions and (d) 0.1 mM L-cysteine by applying a 300 s potential-step electrolysis from 1.1 to 0 V. The HOPG substrates were subjected to electrooxidative pretreatment prior to the electrodeposition of the Au nanoparticles by sweeping the potential for three cycles between  $-1.0$  and  $+2.0 \text{ V vs Ag/AgCl/KCl(sat)}$  in  $N_2$ -saturated 0.5 M  $H_2SO_4$ .

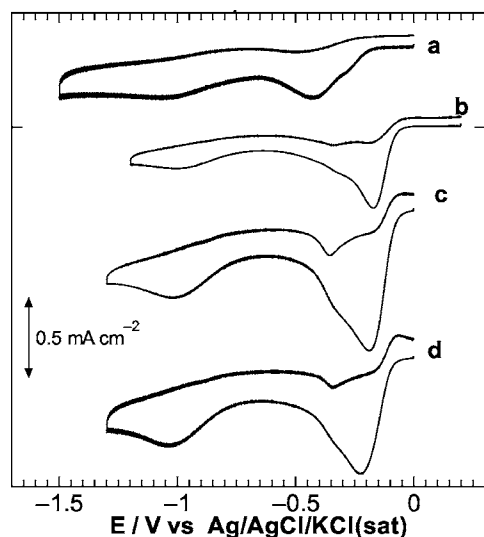


**Figure 10.** CVs for the ORR at (a) pretreated HOPG and (b–d) Au nanoparticles electrodeposited onto pretreated HOPG substrate, measured in  $O_2$ -saturated 0.5 M KOH at potential scan rate of  $100 \text{ mV s}^{-1}$ . The Au nanoparticles were electrodeposited from acidic solution of 0.5 M  $H_2SO_4$  containing 1.0 mM  $Na[AuCl_4]$  in (b) the absence and the presence of (c) 0.1 mM  $I^-$  ions and (d) 0.1 mM L-cysteine by applying a 300 s potential-step electrolysis from 1.1 to 0 V. The HOPG substrates were subjected to electro-oxidative pretreatment prior to the electrodeposition of the Au nanoparticles by sweeping the potential for 60 cycles between  $-1.0$  and  $+2.0 \text{ V}$  vs  $Ag/AgCl/KCl(sat)$  in  $N_2$ -saturated 0.5 M  $H_2SO_4$ .

the presence of iodide ions) (see Table I). Figure 9 and 10 show the effect of the extent of the electro-oxidative pretreatment on the electrocatalytic activity of the electrodeposited Au nanoparticles. Figure 9 shows that the mild electro-oxidative pretreatment of the HOPG substrate has no significant effect on the electrocatalytic activity of the electrodeposited Au nanoparticles. That is, an almost similar CV response was obtained for the ORR at the Au nanoparticles electrodeposited on the untreated and the mildly pretreated HOPG electrodes. Interestingly, Fig. 10 shows a noticeable significant improvement of electrocatalytic activity of the Au nanoparticles electrodeposited on the severely electro-oxidized HOPG substrates toward the ORR, i.e., the positive shift of the cathodic peak potential was observed with an enlargement of the cathodic peak current and the disappearance of the anodic peak. In addition, an inverted peak during the anodic potential scan was found for the Au nanoparticles electrodeposited onto the pretreated HOPG electrodes in the presence of either iodide ions or L-cysteine (see curves c and d of Fig. 10). The morphology of the Au nanoparticles electrodeposited in this case is close to that of Au nanoparticles obtained on the GC electrodes. Also, the Au nanoparticles electrodeposited in the presence of L-cysteine on either GC or the pretreated HOPG electrodes showed the smallest peak intensity at  $2\theta$  of ca.  $38^\circ$  corresponding to the less active Au(111) domains (see curve f of Fig. 4A and curve c of Fig. 5). Thus, it is presumed that the electro-oxidative pretreatment of the HOPG substrates significantly affects the electrocatalytic activity for the ORR of the Au nanoparticles electrodeposited on them. The pretreatment employed in this study is thought to increase the surface hydrophilicity of the HOPG through the generation of some hydrophilic functional groups such as quinone, hydroxy, and carboxylic acid groups on the HOPG surface, while retaining its bulk crystallinity. This leads to the electrodeposition of Au nanoparticles with a high electrocatalytic activity, similar to those electrodeposited on the GC electrode.

### Conclusions

Au nanoparticles with different morphologies have been electrochemically prepared on different substrates in the presence of some

additives like L-cysteine and iodide ions. The nature of the substrates was found to have a direct influence on the morphology, crystallinity, and in turn the electrocatalytic activity of the Au nanoparticles electrodeposited on them. Au nanoparticles with a homogeneously small particle size down to 10 nm were obtained in the presence of iodide ions regardless of the substrates used. The morphology of the Au nanoparticles prepared in the presence of L-cysteine was found to depend primarily on the nature of the substrate. The thus-prepared Au nanoparticles showed a broad spectrum of electrochemical behavior toward the ORR, ranging from a quasi-reversible two-electron reaction to an irreversible four-electron reaction.

### Acknowledgments

This work was financially supported by the Advanced Research Project of Matsushita Electric Industrial Company, Limited, and by Grants-in-Aid for Scientific Research on Priority Areas (no. 417), Scientific Research (no. 12875164 and 14050038), and "Scientific Research (A)" (no. 10305064) from the Ministry of Education, Culture, Sports, Science and Technology, Japan. The authors thank Dr. H. Hashimoto and Dr. Y. Umetani at Matsushita Techno-Research, Incorporated, for their support in the XRD measurements of the Au nanoparticles electrodeposited onto various substrates.

Tokyo Institute of Technology assisted in meeting the publication costs of this article.

### References

1. *Catalysis and Electrocatalysis at Nanoparticle Surfaces*, A. Wieckowski, E. R. Savinova, and C. G. Vayenas, Editors, Marcel Dekker, New York (2003).
2. M. S. El-Deab, T. Sotomura, and T. Ohsaka, *Electrochem. Commun.*, **7**, 29 (2005).
3. M. S. El-Deab and T. Ohsaka, *Electrochim. Acta*, **47**, 4255 (2002).
4. A. K. Gupta and M. Gupta, *Biomaterials*, **26**, 3995 (2005).
5. A. P-Fink, M. Chastellain, L. J-Jeanneret, A. Ferrari, and H. Hofmann, *Biomaterials*, **26**, 2685 (2005).
6. S. Li, W. Yang, M. Chen, J. Gao, J. Kang, and Y. Qi, *Mater. Chem. Phys.*, **90**, 262 (2005).
7. Y. Hida and H. Kozuka, *Thin Solid Films*, **476**, 264 (2005).
8. C. Luo, Y. Zhang, and Y. Wang, *J. Mol. Catal. A: Chem.*, **299**, 7 (2005).
9. A. D. Sarkar and B. C. Khanra, *J. Mol. Catal. A: Chem.*, **299**, 25 (2005).
10. H. Huang and X. Yang, *Colloids Surf., A*, **255**, 11 (2005).
11. Y. Kobayashi, Y. Tadaki, D. Nagao, and M. Konno, *J. Colloid Interface Sci.*, **283**, 601 (2005).
12. H. M. Lu, Z. Wen, and Q. Jiang, *Chem. Phys.*, **309**, 303 (2005).
13. Q. Fu, W. Deng, H. Saltsburg, and M. F-Stephanopoulos, *Appl. Catal., B*, **56**, 57 (2005).
14. S. Kishore, J. A. Nelson, J. H. Adair, and P. C. Eklund, *J. Alloys Compd.*, **389**, 234 (2005).
15. G. Lu, D. Ji, G. Qian, Y. Qi, X. Wang, and J. Suo, *Appl. Catal., A*, **280**, 175 (2005).
16. G. C. Bond and D. T. Thompson, *Catal. Rev. - Sci. Eng.*, **41**(3&4), 319 (1999).
17. S. K. Ghosh, M. Mandal, S. Kundu, S. Nath, and T. Pal, *Appl. Catal., A*, **268**, 61 (2004).
18. S. G. Penn, L. He, and M. J. Natan, *Current Opinion in Chem. Biol.*, **7**, 609 (2003).
19. N. Pradhan, A. Pal, and T. Pal, *Colloids Surf., A*, **196**, 247 (2002).
20. M. Haruta and M. Date, *Appl. Catal., A*, **222**, 427 (2001).
21. M. Kralik and A. Biffis, *J. Mol. Catal. A: Chem.*, **177**, 113 (2001).
22. R. S. Mulukutla, T. Shido, K. Asakura, and Y. Iwasawa, *Scr. Mater.*, **44**, 1695 (2001).
23. H. Yang, C. Coutanceau, J.-M. Leger, N. A.-Vante, and C. Lamy, *J. Electroanal. Chem.*, **576**, 305 (2005).
24. H. Wang, Y. Huang, Z. Tan, and X. Hu, *Anal. Chim. Acta*, **526**, 13 (2004).
25. F. J. V-Iglesias, J. S.-Gullon, P. Rodriguez, E. Herrero, V. Montiel, J. M. Feliu, and A. Aldaz, *Electrochem. Commun.*, **6**, 1080 (2004).
26. O. V. Cherstouk, P. A. Simonov, and E. R. Savinova, *Electrochim. Acta*, **48**, 3851 (2003).
27. Y. Zhang, S. Asahina, S. Yoshihara, and T. Shirakashi, *Electrochim. Acta*, **48**, 741 (2003).
28. I. Yagi, T. Ishida, and K. Uosaki, *Electrochem. Commun.*, **6**, 773 (2004).
29. M. S. El-Deab, T. Okajima, and T. Ohsaka, *J. Electrochem. Soc.*, **150**, A851 (2003).
30. M. S. El-Deab and T. Ohsaka, *J. Electroanal. Chem.*, **553**, 107 (2003).
31. M. S. El-Deab and T. Ohsaka, *Electrochem. Commun.*, **4**, 288 (2002).
32. S. Schimpf, M. Lucas, C. Mohr, U. Rodemerck, A. Bruckner, J. Radnik, H. Hofmeister, and P. Calus, *Catal. Today*, **72**, 63 (2002).
33. M. Haruta, *Catal. Today*, **36**, 153 (1997).
34. M. O. Finot, G. D. Braybrook, and M. T. McDermott, *J. Electroanal. Chem.*, **466**, 234 (1999).
35. M. S. El-Deab, T. Sotomura, and T. Ohsaka, *J. Electrochem. Soc.*, **152**, C1 (2005).
36. J. Jiang and A. Kucernak, *Electrochim. Acta*, **47**, 2381 (2002).
37. C. C. Hu and T. W. Tsou, *Electrochim. Acta*, **47**, 3523 (2002).

38. C. C. Hu and T. W. Tsou, *Electrochem. Commun.*, **4**, 105 (2002).
39. M.-S. Wu and P.-C. J. Chiang, *Electrochem. Solid-State Lett.*, **7**, A123 (2004).
40. H. Y. Lee, S. W. Kim, and H. Y. Lee, *Electrochem. Solid-State Lett.*, **4**, A19 (2001).
41. M. S. Hong, S. H. Lee, and S. W. Kim, *Electrochem. Solid-State Lett.*, **5**, A227 (2002).
42. S. C. Pang, M. A. Anderson, and T. W. Chapman, *J. Electrochem. Soc.*, **147**, 444 (2000).
43. S. C. Pang and M. A. Anderson, *J. Mater. Res.*, **15**, 2096 (2000).
44. S. F. Chin, S. C. Pang, and M. A. Anderson, *J. Electrochem. Soc.*, **149**, A379 (2002).
45. V. Srinivasan and J. W. Weidner, *J. Electrochem. Soc.*, **144**, L210 (1997).
46. E. Budevski, G. Staikov, and W. J. Lorenz, *Electrochemical Phase Formation and Growth*, Chap. 4, VCH, Weinheim (1996).
47. F. Gao, M. S. El-Deab, T. Okajima, and T. Ohsaka, *J. Electrochem. Soc.*, **152**, A1226 (2005).
48. A. Chen, Z. Chi, D. Bizzotto, J. Lipkowski, B. Pettinger, and C. Bilger, *J. Electroanal. Chem.*, **467**, 342 (1999).
49. K. S. Wilson and A. J. Rogers, *Tech. Proc. American Electroplaters Soc.*, **51**, 92 (1964).
50. K. Inoue, T. Nakata, Y. Shindo, and T. Watanabe, *J. Jpn. Inst. Met.*, **66**, 400 (2002).
51. M. S. El-Deab, K. Arihara, and T. Ohsaka, *J. Electrochem. Soc.*, **151**, E213 (2004).